1990年度 大韓醫用生體工學 秋季 學術大會 論文集 90/11

복부 핵자기공명 영상에서 영상번짐의 교정을 위한 최적 호흡 정렬법

°정 관 진, 안 우 연, 조 장 희
한국과학기술원 전기 및 전자공학과

Optimal Respiratory Ordering Scheme (*OROS*) for Correcting Blurring Artifacts in Abdominal Magnetic Resonance Imaging

°Kwan Jin Jung, Woo Youn Ahn, and Zang Hee Cho
Dept. of Electrical Engineering, Korea Advanced Institute of Science and Technology

Abstract

In abdominal NMR imaging the respiratory ordering techniques have been successfully used to remove the ghosting artifacts arising from the respiratory motion. In the existing respiratory ordering schemes, however, it is generally accepted that blurring of the moving parts still remains as in the signal averaging technique. A new optimal respiratory ordering scheme which can correct the blurring as well as the ghosting artifacts is theoretically derived through the analysis of the phase encoding directional motion effects in Fourier imaging. The performance of the optimal respiratory ordering scheme is experimentally confirmed together with a suboptimal ordering scheme which is suggested as a compromise for the practicality.

I. Introduction

In abdominal imaging the respiratory motion artifacts appear as blurring of the moving parts and multiple ghosts smeared in the phase encoding direction in 2-D Fourier imaging (*1*). Many techniques such as respiratory gating, ROPE (respiratory ordered phase encoding), and signal averaging have been developed to reduce the motion artifacts of ghosts and blurs (*1, 2*). Respiratory gating and ROPE techniques require respiratory monitoring which can be done by the additional hardware or the acquisition of the projection profile (*3*). The gating technique is seen to be ideal in the same way as the cardiac gating, but it needs more scan time and the irregular respiratory cycle may cause the signal variation as in the cardiac gating (*4 - 6*). The ROPE technique can eliminate the ghosting artifacts (*7*), but is known to still cause blurring of the moving part (*1, 2, 8, 9*).

Through the theoretical analysis of the phase encoding directional motion effects, it is newly found that there exists an optimal respiratory ordering scheme of the phase encoding gradient which can correct the blurring of the moving parts in contrast to the allowed blurring in the previously reported versions of the ordering scheme.

II. Methods

The effects of the periodic motion in the phase encoding direction are analyzed for Fourier transform imaging. Based on the analysis the optimal and suboptimal respiratory ordering schemes are proposed along with the simulation results.

1. Analysis of Motion-Affected Blur

All kinds of irregular motions are known to produce the motion artifacts of ghosts and blurs (*6, 10- 12*). Usually the phase encoding direction of 2-D Fourier imaging is aligned with the breathing motion direction, therefore the following analysis is performed only for the phase encoding directional motion.

In 2-D Fourier imaging the NMR signal is expressed by the Fourier transform relationship

$$S(\omega_x,\omega_y) = \int_{-L_y/2}^{L_y/2}\int_{-L_x/2}^{L_x/2} \rho(x,y)\exp[-i(x\omega_x + y\omega_y)]\,dx\,dy, \quad [1]$$

where L_x and L_y are the x and y directional field-of-views, respectively (13). For the simplicity let us assume an 1-D object distributed only in the phase encoding or y direction while the readout gradient is assumed to be in the x direction, i.e.,

$$\rho(x,y) = \delta(x)\,\rho(y). \quad [2]$$

From Eqs. [1] and [2] the NMR signal of the 1-D object is expressed as a function of the phase encoding frequency ω_y, i.e.,

$$S(\omega_y) = \int_{-L_y/2}^{L_y/2} \rho(y)\exp(-iy\omega_y)\,dy. \quad [3]$$

When the 1-D object of the finite size L_v is centered at $y = y_0$ with a uniform distribution, i.e.,

$$\rho(y) = \begin{cases} 1 \text{ for } -L_v/2 \le (y - y_0) \le L_v/2 \\ 0 \text{ elsewhere} \end{cases} \quad [4]$$

the NMR signal of the stationary object, i.e., y_0 = constant, becomes

$$S(\omega_y) = L_v\,\mathrm{sinc}\left(\frac{L_v}{2\pi}\omega_y\right)\exp(-i\omega_y y_0) \quad [5]$$

from Eqs. [3] and [4]. But, when the object moves during the image scan time, the moving object's center position y_c can be expressed as a function of the phase encoding frequency ω_y, i.e.,

$$y_c(\omega_y) = y_0 + y_v(\omega_y), \quad [6]$$

where $y_v(\omega_y)$ is the relative displacement from a reference center position y_0. Substituting $y_c(\omega_y)$ for y_0 into Eq. [5], the NMR signal becomes

$$S(\omega_y) = L_v\,\mathrm{sinc}\left(\frac{L_v}{2\pi}\omega_y\right)\exp(-i\omega_y y_0)\exp[-i\omega_y y_v(\omega_y)], \quad [7]$$

where the motion during the data acquisition and the motion-induced phase shift are neglected since the motion-induced phase shift can be nullified by applying the motion gradients (*14 - 16*). The last term in Eq. [7] contains the information of the motion artifacts and therefore is designated as an artifact function $B(\omega_y)$, i.e.,

$$B(\omega_y) = \exp[-i\omega_y y_v(\omega_y)]. \quad [8]$$

The effects of the artifact function on the resultant image can be studied by modeling the object motion as a sinusoidal motion which is periodic with the angular frequency ω (*8, 10*). When the phase encoding gradient is assumed to be ordered linearly, i.e.,

$$n = -N_c/2, \ldots, -1, 0, 1, \ldots, (N_c/2 - 1), \quad [9]$$

the motion can be expressed as a function of the phase encoding step number n, i.e.,

$$y_v(n) = -\alpha\sin[\omega(N_c/2 + n)T_R + \theta] = -\alpha\sin(\omega T_R n + \theta'), \quad [10]$$

where N_c is the number of the phase encoding steps; α is the maximum motion displacement in the pixel unit; T_R is the pulse repetition time; and θ is an arbitrary phase of the sinusoidal motion. By using the relationship $\omega_y = n\gamma g_c T_c$, where g_c and T_c are the step amplitude and pulse duration of the phase encoding gradient, Eq [10] can be expressed as a function of the phase encoding frequency ω_y, i.e.,

$$y_v(\omega_y) = -\alpha \sin(\omega \frac{T_R}{\gamma g_c T_c}\omega_y + \theta') = -\alpha \sin(b\omega_y + \theta'), \quad [11]$$

where $\theta' = \theta + \omega\frac{N_c}{2}T_R$ and $b = \omega\frac{T_R}{\gamma g_c T_c}$.

Substituting the expression for $y_v(\omega_y)$ into Eq. [8], the artifact function $B(\omega_y)$ becomes

$$B(\omega_y) = \exp[i\alpha\omega_y \sin(b\omega_y + \theta')] \quad [12]$$

and can be expanded in a series form (*8, 10*)

$$B(\omega_y) = \sum_{k=-\infty}^{\infty} J_k(\alpha\omega_y)\exp[ik(b\omega_y + \theta')] \quad [13]$$

or

$$B(\omega_y) = J_0(\alpha\omega_y) + \sum_{k=1}^{\infty} J_k(\alpha\omega_y)\{\exp[ik(b\omega_y+\theta')] + (-1)^k\exp[-ik(b\omega_y+\theta')]\}, \quad [14]$$

where J_k is the kth order Bessel function of the first kind and in arriving at Eq. [14] the Bessel identity $J_{-k}(x) = (-1)^k J_k(x)$ is used (*17*). The implications of the artifact function can be better understood through computer simulations. Bessel functions $J_k(\alpha\omega_y)$ for $k = 0$, 1, and 2 are plotted in Fig. 1(a) for $\alpha =$ 10 pixel and Fourier transforms of $J_0(\alpha\omega_y)$ is shown in Fig. 1(b). The Fourier transform of $J_k(\alpha\omega_y)$ tells how it will blur the moving object by the convolution process in the spatial domain, while $J_k(\alpha\omega_y)$ for $k \neq 0$ corresponds to each pair of ghosts shifted away from the original position by $\pm kb$ with blurring and amplitude scaling determined by $J_k(\alpha\omega_y)$.

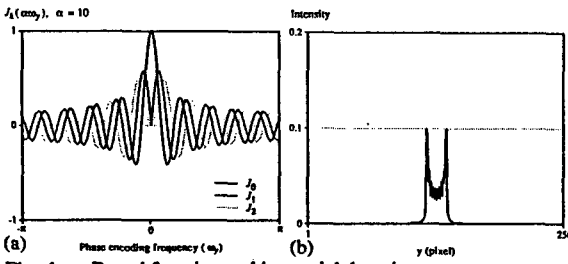

Fig. 1. Bessel function and its spatial domain response. (a) Bessel function $J_k(\alpha\omega_y)$ plotted as a function of the phase encoding frequency ω_y for α = 10 pixel. (b) Fourier transforms of $J_0(\alpha\omega_y)$ for $\alpha = 10$.

2. *Optimal Respiratory Ordering Scheme (OROS)*

In ROPE or COPE (centrally ordered phase encoding) techniques (*7, 8*) the phase encoding steps have been ordered in consideration of the physical respiratory motion so that the respiratory motion appears to be effectively slow-varying along the phase encoding frequency ω_y in such patterns as half- or full-cycle sinusoidal curves. Thereby the ghosts can have been successfully suppressed, but there still exists significant blurring of the moving part. When the half-cycle sinusoidal ordering scheme of the relationship

$$y_v(\omega_y) = \alpha \sin(\omega_y/2), \quad -\pi \le \omega_y < \pi \quad [15]$$

is applied for the moving object with the displacement of 10 pixel, i.e., $\alpha = 10$, as illustrated in Fig. 2(a), no ghost occurs as known, but the object is blurred or dispersed at the original position as shown in Fig. 2(b).

In principle, the motion artifacts can be removed if the artifact function $B(\omega_y)$ of Eq. [8] can be made to be independent of the phase encoding frequency ω_y by imposing the relationship

$$y_v(\omega_y) = \frac{c}{\omega_y} \quad [16]$$

for any constant c except $c = 0$. In other words, if the phase encoding frequency is ordered to have the inverse relationship with the motion displacement, the moving object can be reconstructed correctly without blurring as well as ghosting artifacts. In this sense the ordering relationship [16] is optimal and is designated as an optimal respiratory ordering scheme. The optimal respiratory ordering scheme and its effects are shown in Figs. 2(c) and 2(d), respectively, where $y_v(\omega_y)$ is set to 0 at $\omega_y = 0$ and c is given for $y_v(\omega_y)$ to be the maximum displacement α at $\omega_y = \pm\pi/128$. In comparison with the severe blurring in Fig. 2(b), the blurring artifacts are clearly corrected and the signal intensity of the moving object is well recovered. When applied to the abdominal imaging, however, the optimal respiratory ordering scheme can only provide a guiding curve for the respiratory ordering due to its discrepancy from the typical respiratory motion pattern (*5*). To improve the practicality a suboptimal respiratory ordering scheme is designed by shifting the coordinate axes of the optimal ordering scheme to satisfy the geometrical constraints $y = 0$ at $\omega_y = \pm\pi$ or 0, and $y = \pm\alpha$ at $\omega_y = \pm\pi/128$. Thus obtained suboptimal ordering scheme plotted in Fig. 2(e) is given by

$$y_v(\omega_y) = \frac{\alpha}{e}\left|\frac{1}{\omega_y + d} - d\right|, \quad [17]$$

where $d = \frac{2}{\pi + \sqrt{\pi^2 + 4}}$ and $e = \frac{1}{\pi/128 + d} - d$.

The spatial response of the suboptimal ordering scheme is inferior to the optimal case as shown in Fig. 2(f) as a result of the discrepancy from the optimal ordering curve.

3. *Computer Simulations*

The three ordering schemes are examined by the computer simulation using a phantom of Fig. 3(a) which is composed of several moving parts with different motion displacements. The motion of each part is assumed to be bulky and synchronized. The simulation results are shown in Figs. 3(b) - 3(d) for the three kinds of ordering schemes. Blurring which is so evident in the sinusoidal ordering scheme is corrected in the optimal ordering scheme except the small background offset which is considered to be caused by the nonlinear phase shift of the artifact function at $\omega_y = 0$. Also it is noteworthy that the intensities of the moving parts are very close to those of the original phantom. In the suboptimal ordering case, the upper edges of the moving parts are well recovered, but there is still some blurring in the lower edges of the moving parts, which is considered to be caused by the nonlinear phase response of the artifact function.

III. Experimental Results

The proposed respiratory ordering schemes were tested experimentally for the abdominal axial slice of a human body using the KAIS 2.0 Tesla whole body NMR imaging system. As reference images for comparing with the following ordering schemes, two images with single- and 30-average are

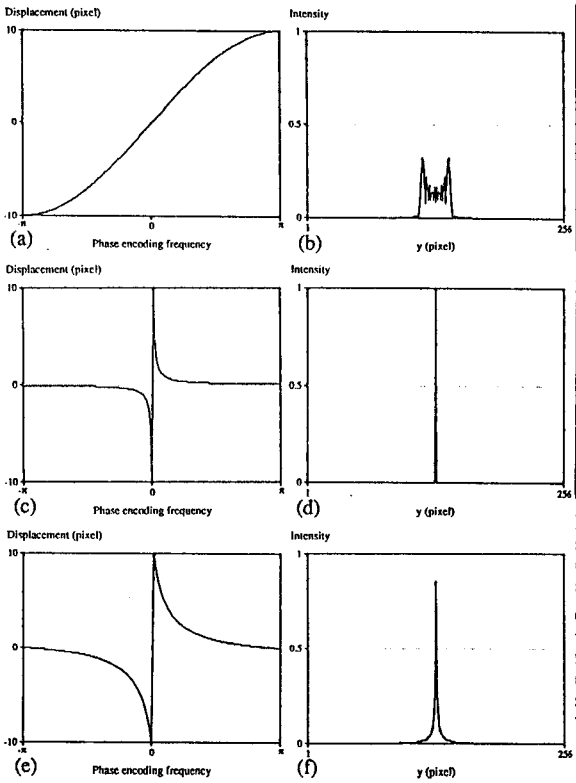

Fig. 2. Three kinds of respiratory ordering schemes and their spatial domain responses for the motion displacement of 10 pixel, i.e., α = 10 pixel.
(a) and (b) Sinusoidal ordering.
(c) and (d) Optimal ordering.
(e) and (f) Suboptimal ordering.

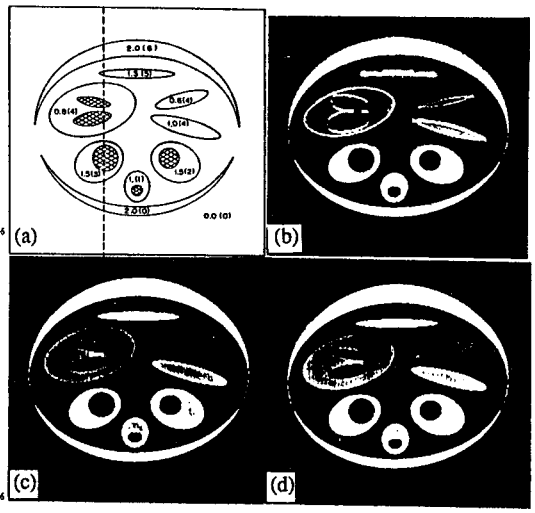

Fig. 3. Computer simulations of the three ordering schemes.
(a) Phantom. The number of each part represents the intensity and the number in the parentheses denotes the motion displacement α of each part in the pixel unit. The dotted vertical line through the phantom represents the position for the cut-view.
(b) - (d) Simulation images for the sinusoidal, optimal, and suboptimal ordering schemes, respectively. The three images were photographed using the same display window level.

shown in Figs. 4(a) and 4(b), respectively. In the single-average case there appear severe motion and flow artifacts. The flow artifacts arise from the inflow and acceleration effects of the pulsatile flow in the aorta and they can be easily eliminated by applying the presaturation technique (*8*). Here, however, the presaturation technique was not applied in order to see the ordering and averaging effects on the flow artifacts at the same time. In the signal averaging case of 30 repetitions most of the ghosts are eliminated and the flow artifacts are cleared up. However, blurring is evident especially in the frontal body wall.

To the same data set the three kinds of ordering schemes were applied, i.e., sinusoidal, optimal, and suboptimal ordering schemes according to the relationships [15], [16], and [17], respectively. In all the ordering cases the ghosting artifacts are greatly suppressed in comparison with the single-average case of Fig. 4(a), but the flow artifacts still remain because the heart cycle is not related with the respiratory motion cycle. The interesting comparison aspect is blurring or the edge sharpness particularly of the frontal body wall. The conventional sinusoidal case of Fig. 4(c) shows severe blurring as in the 30-average case of Fig. 4(b) even though the employed displacement range is narrower than the other two cases. In contrast, the optimal ordering case of Fig. 4(d) provides very clear edges as proposed and the suboptimal case of Fig. 4(e) shows much less blurring than the conventional sinusoidal one even though it is inferior to the optimal case.

VI. Conclusions

Blurring artifacts which have been known to be inevitable in the existing respiratory ordering schemes can now be corrected by the optimal respiratory ordering scheme. The optimal respiratory ordering scheme is theoretically derived through the analysis of the phase encoding directional motion effects in 2-D Fourier imaging. The optimal ordering scheme is again modified to the suboptimal ordering scheme to improve the practicality with the penalty of the imperfect correction of the blurring artifacts. Through computer simulations and experiments the blurring artifacts are clearly corrected in the optimal case and sufficiently corrected in the suboptimal case. The suboptimal ordering scheme needs to be improved further for the better compromise between the blurring and the practicality. The discovery of the respiratory ordering scheme without the blurring artifacts is expected to renew the value of the respiratory ordering technique as an efficacious solution to the blurring as well as the ghosting artifacts arisen from the respiratory motion even though more scan time is needed.

References

1. M. L. Wood and R. M. Henkelman, "Suppression of Respiratory Motion Artifacts in Magnetic Resonance Imaging," *Med. Phys.* 13(6), 794-805 (1986).
2. V. M. Runge and M. L. Wood, "Fast Imaging and Other Motion Artifact Reduction Schemes: A Pictorial Overview," *Magn. Reson. Imaging* 6, 595-608 (1988).

3. J. J. M. Cuppen, J. P. Groen, J. J. E. In den Kleef, and H. A. Tuithof, "Reduction of Motion Artifacts by Data Postprocessing," *in* Abstracts, 4th Annual Meeting of *SMRM*, 962-963, 1985.
4. V. M. Runge, J. A. Clanton, C. L. Partain, A. E. Jr. James, "Respiratory Gating in Magnetic Resonance Imaging at 0.5 Tesla," *Radiology* **151**, 521-523 (1984).
5. R. L. Ehman, M. T. McNamara, M. Pallack, H. Hricak, and C. B. Higgins, "Magnetic Resonance Imaging with Respiratory Gating: Techniques and Advantages," *Amer. J. Roentgenol.* **143**, 1175-1182 (1984).
6. C. L. Schultz, R. J. Alfidi, A. D. Nelson, S. Y. Kopiwoda, and M. E. Clampitt, "The Effect of Motion on Two-Dimensional Fourier Transformation Magnetic Resonance Images," *Radiology* **152**, 117-121 (1984).
7. D. R. Bailes, D. J. Gilderdale, G. M. Bydder, A. G. Collins, and D. N. Firmin, "Respiratory Ordered Phase Encoding (ROPE): A Method for Reducing Respiratory Motion Artefacts in MR Imaging," *J. Compt. Assist. Tomogr.* 9(4), 835-838 (1985).
8. E. M. Haacke and J. L. Patrick, "Reducing Motion Artifacts in Two-Dimensional Fourier Transform Imaging," *Magn. Reson. Imaging* **4**, 359-376 (1986).
9. G. E. Wesby, R. R. Edelman, and R. Harris, "Artifacts in MR Imaging: Description, Causes, and Solutions," *in* Clinical Magnetic Resonance Imaging (R. R. Edelman, J. R. Hesselink, Eds.), Part. 1, p. 100, Saunders, Philadelphia, 1990.
10. M. L. Wood and R. M. Henkelman, "MR Image Artifacts from Periodic Motion," *Med. Phys.* **12**, 143-151 (1985).
11. L. Axel, R. M. Summers, H. Y. Kressel, and C. Charles, "Respiratory Effects in Two-Dimensional Fourier Transform MR Imaging," *Radiology* **160**, 795-801 (1986).
12. V. J. Wedeen, R. E. Wendt III, and M. Jerosch-Herold, "Motional Phase Artifacts in Fourier Transform MRI," *Magn. Reson. Med.* **11**, 114-120 (1989).
13. Z. H. Cho, "Computerized Tomography," *in* Encyclopedia of Physical Science and Technology, Vol. 3, 507-544, Academic Press, 1987.
14. P. M. Pattany, J. J. Phillips, L. C. Chiu, J. D. Lipcamon, J. L. Duerk, J. M. McNally, and S. N. Mohapatra, "Motion Artifact Suppression Technique (MAST) for MR Imaging," *J. Compt. Assist. Tomogr.* 11(3), 369-377 (1987).
15. E. M. Haacke and G. W. Lenz, "Improving MR Image Quality in the Presence of Motion by Using Rephasing Gradients," *Amer. J. Roentgenol.* **148**, 1251-1258 (1987).
16. P. J. Keller and F. W. Wehrli, "Gradient Moment Nulling through the Nth Moment: Application of Binomial Expansion Coefficients to Gradient Amplitudes," *J. Magn. Reson.* **78**, 145-149 (1988).
17. G. Arfken, "Mathematical Methods for Physicists," 3rd Ed., Ch. 11, Academic Press, Orlando, 1985.

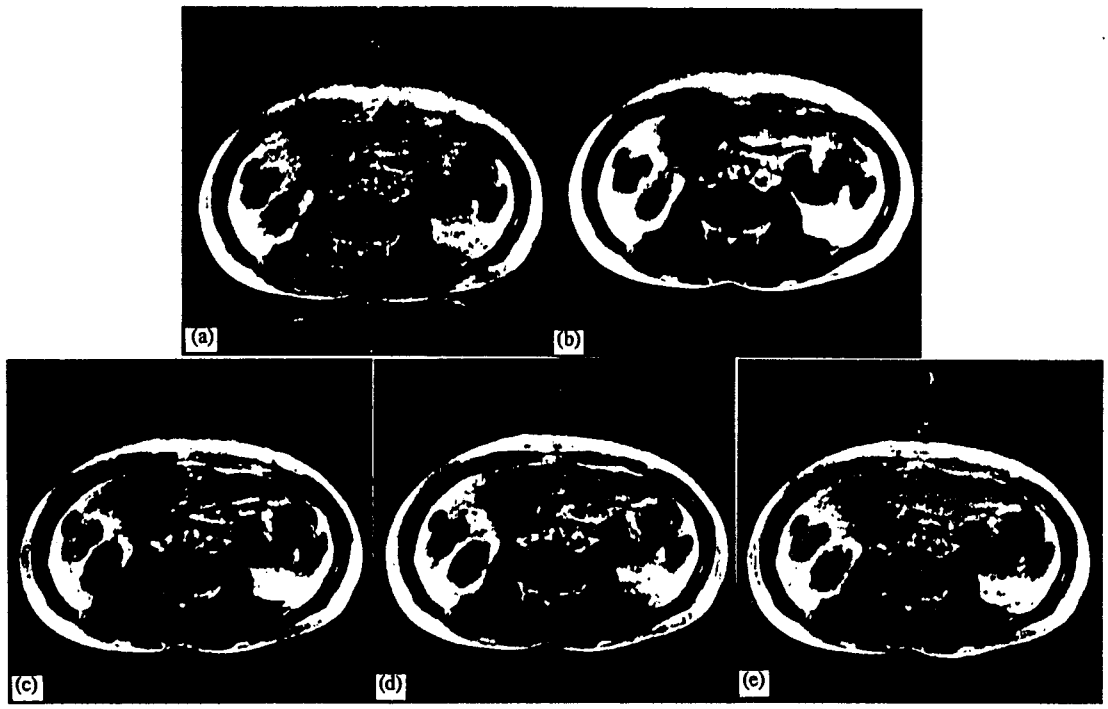

Fig. 4. Axial slice images of a human body. Imaging conditions were field-of-view = 300 mm, slice thickness = 10 mm, T_R/T_E = 200/34 ms, number of phase encoding step = 120, number of repetition at each phase encoding steps = 30, and image matrix size = 256 x 256. The photographs were taken using the same display window setting.
(a) and (b) Single- and 30-average. (c) sinusoidal, (d) optimal, and (e) suboptimal ordering schemes.